CORE
Metadata, citation and similar papers at core.ac.uk
Provided by Archivio istituzionale della ricerca - Università di Palermo

Frictionless contact-detachment analysis: iterative linear complementarity and quadratic programming approaches

M. Salerno, S. Terravecchia & L. Zito

Computational Mechanics
Solids, Fluids, Structures, Fluid-Structure Interactions, Biomechanics, Micromechanics, Multiscale Mechanics, Materials, Constitutive Modeling, Nonlinear Mechanics, Aerodynamics

ISSN 0178-7675
Volume 51
Number 4

Comput Mech (2013) 51:553-566
DOI 10.1007/s00466-012-0752-4

Springer

Your article is protected by copyright and all rights are held exclusively by Springer-Verlag. This e-offprint is for personal use only and shall not be self-archived in electronic repositories. If you wish to self-archive your work, please use the accepted author's version for posting to your own website or your institution's repository. You may further deposit the accepted author's version on a funder's repository at a funder's request, provided it is not made publicly available until 12 months after publication.

Springer

Author's personal copy

Comput Mech (2013) 51:553–566
DOI 10.1007/s00466-012-0752-4

ORIGINAL PAPER

Frictionless contact-detachment analysis: iterative linear complementarity and quadratic programming approaches

M. Salerno · S. Terravecchia · L. Zito

Received: 8 February 2012 / Accepted: 14 June 2012 / Published online: 5 July 2012
© Springer-Verlag 2012

Abstract The object of the paper concerns a consistent formulation of the classical Signorini's theory regarding the frictionless contact problem between two elastic bodies in the hypothesis of small displacements and strains. The employment of the symmetric Galerkin boundary element method, based on boundary discrete quantities, makes it possible to distinguish two different boundary types, one in contact as the zone of potential detachment, called the real boundary, the other detached as the zone of potential contact, called the virtual boundary. The contact-detachment problem is decomposed into two sub-problems: one is purely elastic, the other regards the contact condition. Following this methodology, the contact problem, dealt with using the symmetric boundary element method, is characterized by symmetry and in sign definiteness of the matrix coefficients, thus admitting a unique solution. The solution of the frictionless contact-detachment problem can be obtained: (i) through an iterative analysis by a strategy based on a linear complementarity problem by using boundary nodal quantities as check quantities in the zones of potential contact or detachment; (ii) through a quadratic programming problem, based on a boundary *min-max* principle for elastic solids, expressed in terms of nodal relative displacements of the virtual boundary and nodal forces of the real one.

M. Salerno (✉)
D.to di Costruzioni e Metodi Matematici in Architettura,
University of Napoli Federico II, Via Toledo 402,
80132 Naples, Italy
e-mail: maria.salerno@unina.it

S. Terravecchia · L. Zito
D.to di Ingegneria Civile, Ambientale e Aerospaziale, University
of Palermo, Viale delle Scienze, 90128 Palermo, Italy
e-mail: silvioterravecchia@gmail.com

L. Zito
e-mail: zitoliborio@tiscali.it.

Keywords Symmetric BEM · Contact-detachment · Linear Complementarity · Quadratic Programming

1 Introduction

After the pioneering work of Signorini [1], the problems of unilateral contact between an elastic body and a rigid obstacle, or between two (impenetrable) elastic bodies, also received great interest within the boundary element approaches [2] at the beginning of the last decade of the past century.

The main difficulty in solving the Signorini problem arises from the fact that the position, where the change takes place from one type of boundary condition to another, is undetermined in advance, with the result that this problem proves to be geometrically non-linear. The solution to this problem can be obtained either through an indirect approach of an iterative kind dealt with using the linear complementarity problem (LCP) [3–6] or through a direct approach as the *min-max* solution of appropriate discrete functionals whose solution requires the employment of quadratic programming problem (QPP) techniques [7–12].

The symmetric Galerkin boundary element method (SGBEM) has been applied to unilateral contact problems by utilizing variational formulations in elasticity and in elastoplasticity [9,10], by using iterative procedures to solve the quadratic programming problem [13], by linear complementarity in an iterative procedure [6,14], by a penalty approximation of the Coulomb law of friction through a symmetric discretization of the Stelklov–Poincaré operator [15] and by putting together the SGBEM and the collocation approach [16].

In this paper a strategy is shown for the solution to the coupled contact-detachment problem using the mixed

Author's personal copy

variable multidomain SGBEM approach. The idea is based on the classical subdivision of the domain into substructures introduced in the SGBEM by some authors [15–22], where a mixed variable approach is utilized.

The multidomain strategy employed here is the same as that in [22], where the governing equation system is obtained by imposing the regularity conditions between substructures regarding the kinematical and mechanical quantities both in terms of nodal variables (strong regularity) and in terms of generalized ones (weak regularity). Through this strategy a single solving equation is obtained in order to solve engineering problems in elasticity. Indeed, in the bodies in contact, considered as substructures, a preliminary boundary discretization is made and a distinction is performed between the boundary in contact but considered as the zone of potential detachment, called the real boundary, and another one, detached, considered as the zone of potential contact, called the virtual boundary. The regularity condition, previously described, gives rise to appropriate algebraic operators able to be utilized for both an indirect approach like the iterative LCP, and a direct approach like the QPP.

Let us now introduce a brief description of the two strategies employed here to solve the contact-detachment problems:

- The first strategy is based on an iterative procedure, starting from the Signorini equations written in an appropriate form in order that the LCP could be applied. In this way the writing of the aforesaid equations is performed by using nodal mechanical and kinematical variables, considered as check quantities on the real and virtual boundaries. This gives rise to an efficient and high-performance strategy able to give a good final response but also a lot of information during the whole contact-detachment process but through a path which is computationally more onerous, because it is based on an iterative procedure, in comparison with direct strategies. The main advantage of this iterative formulation is that the algebraic operators governing the contact-detachment problem, symmetric and in sign definite, does not need to be re-computed when the contact and detached boundaries change typologically since some row and column blocks modify their collocation in the iterative process.
- The second one is based on the solution obtained through a QPP as a *min-max* problem of a reduced functional having only nodal mechanical and kinematical interface variables or of two independent subproblems of *min* and of *max* of two functionals able to perform separately the contact and detachment solution with very low computational burdens and CPU times. The QPP approach proves to be very advantageous in terms of computational burdens but unable to furnish information during the contact-detachment process.

These approaches show a more rational and innovatory strategy regarding both the iterative LCP and the QPP procedures obtained using the multidomain symmetric BEM, like using the same algebraic operators in both the procedures in the analysis process.

Some examples regarding the contact-detachment phenomenon are considered and some comparisons between the solutions with the iterative LCP analysis and the direct QPP approach will be shown, and also comparisons with other authors.

2 Mixed variable multidomain approach

This section shows the procedure utilized to obtain, using the mixed variable multidomain approach of the symmetric BEM, an equation connecting mechanical and kinematical weighted quantities in the boundaries to mechanical and kinematical nodal quantities defined in the same boundaries, and to the known boundary (forces and imposed displacements) and domain (body forces) actions. This expression is characterized by elastic operators containing the geometry and constitutive data.

Consider the classical Somigliana Identities (S.Is.) i.e.:

$$\mathbf{u} = \int_{\Gamma} \mathbf{G}_{uu}\mathbf{f}d\Gamma + \int_{\Gamma} \mathbf{G}_{ut}(-\mathbf{u})d\Gamma + \int_{\Omega} \mathbf{G}_{uu}\,\overline{\mathbf{b}}\,d\Omega \tag{1a}$$

$$\mathbf{t} = \int_{\Gamma} \mathbf{G}_{tu}\mathbf{f}d\Gamma + \int_{\Gamma} \mathbf{G}_{tt}(-\mathbf{u})\,d\Gamma + \int_{\Omega} \mathbf{G}_{tu}\overline{\mathbf{b}}\,d\Omega \tag{1b}$$

These provide the displacements and tractions in Ω caused by layered mechanical jumps $\mathbf{f}$ and double-layered kinematical ones $-\mathbf{u}$, both known and unknown boundary vectors, as well as by body forces $\overline{\mathbf{b}}$ in the Ω domain. The operators $\mathbf{G}_{pq}$ are the Fundamental Solution matrices in which, on the basis of the symbology introduced by Maier and Polizzotto [23], the subscripts $p = u, t, \sigma$ and $q = u, t, \sigma$ indicate the effect (u displacement, t traction) and the dual quantity in an energetic sense (u force, t displacement) associated with the cause, respectively.

The analysis process concerns two bodies in contact subjected to external actions, constant or variable in time in a quasi-static way (Fig. 1). The problem appears nonlinear because the external actions modify the contact area that characterizes the boundaries of the two bodies, modifying the free boundary into a contact one and vice versa.

To this aim, in this paper, a strategy has been developed to use two types of analysis, i.e. the LCP and QPP, through the use of the same algebraic operators that govern the contact-detachment phenomenon.

Let the homogeneous elastic two-dimensional bodies A and B of domains Ω^A and Ω^B, supposed to be in contact with one another along a portion of boundary, be subjected

Author's personal copy

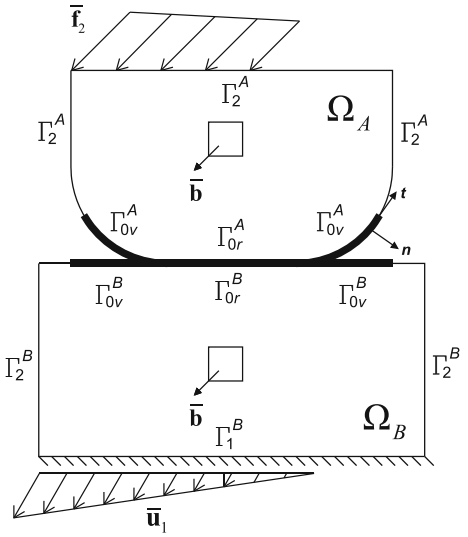

Fig. 1 System subdivided into the BEM-elements A and B

to external actions (Fig. 1). Let the boundary of each body be distinguished into constrained Γ_1, free Γ_2, real interface Γ_{0r} and virtual interface Γ_{0v}, $\Gamma_0 = \Gamma_{0r} \cup \Gamma_{0v}$ being the boundary where the contact-detachment phenomenon takes place [13]. In detail the real interface boundary Γ_{0r} is the real contact zone between the solids A and B characterized by the possibility of changing typologically into a free type boundary after the detachment analysis. Vice versa the virtual interface boundary Γ_{0v} is a free type boundary that can change typologically into a contact one. The subdivision between these two boundary types of the elastic solids is performed beforehand.

Each of the two bodies A and B is subjected to in-plane actions: forces $\bar{\mathbf{f}}_2$ at the portion Γ_2 of the free boundary, displacements $\bar{\mathbf{u}}_1$ imposed at the portion Γ_1 of the constrained boundary, and body force $\bar{\mathbf{b}}$ in Ω.

The contact-detachment between the two bodies involves the presence of the boundary $\Gamma_0 = \Gamma_{0r} \cup \Gamma_{0v}$ in each of them, but no action can be applied.

We want to obtain the length of the boundary which has modified its status (in contact or detached) and, for each body, the elastic response to the external actions in terms of displacements $\mathbf{u}_2$ on Γ_2 and reactive forces $\mathbf{f}_1$ on Γ_1, but also in terms of the displacements $\mathbf{u}_{0v}$ and tractions $\mathbf{t}_{0v}$ (the latter vector null by definition) on the virtual boundary Γ_{0v}, displacements $\mathbf{u}_{0r}$ and tractions $\mathbf{t}_{0r}$ at the real boundary Γ_{0r} and in terms of stresses $\boldsymbol{\sigma}$ in the domain of each body by using the mixed variable multidomain SGBEM approach [16–22].

2.1 Elastic equation of each body

Consider a body, here called BEM-element (BEM-e), characterized by the boundary Γ distinguished into four parts, free Γ_2, constrained Γ_1, virtual interface Γ_{0v} and real interface Γ_{0r} boundaries. For this BEM-e the following Dirichlet and Neumann conditions can be written:

$$\begin{aligned} &\mathbf{u}_1 = \bar{\mathbf{u}}_1 \quad \text{on } \Gamma_1 \\ &\mathbf{t}_2 = \bar{\mathbf{f}}_2 \quad \text{on } \Gamma_2 \end{aligned} \tag{2a, b}$$

If in the latter equations we introduce the S.Is. of the displacements and tractions of Eqs. (1a, b), the following boundary integral equations can be written:

$$\begin{aligned} &\mathbf{u}_1\left[\mathbf{f}_1, -\mathbf{u}_2, \mathbf{f}_{0r}, -\mathbf{u}_{0r}, \mathbf{f}_{0v}, -\mathbf{u}_{0v}\right] + \mathbf{u}_1\left[\bar{\mathbf{f}}_2, -\bar{\mathbf{u}}_1^{CPV}, \bar{\mathbf{b}}\right] \\ &\quad + \frac{1}{2}\bar{\mathbf{u}}_1 = \bar{\mathbf{u}}_1 \\ &\mathbf{t}_2\left[\mathbf{f}_1, -\mathbf{u}_2, \mathbf{f}_{0r}, -\mathbf{u}_{0r}, \mathbf{f}_{0v}, -\mathbf{u}_{0v}\right] + \mathbf{t}_2\left[\bar{\mathbf{f}}_2^{CPV}, -\bar{\mathbf{u}}_1, \bar{\mathbf{b}}\right] \\ &\quad + \frac{1}{2}\bar{\mathbf{f}}_2 = \bar{\mathbf{f}}_2 \end{aligned} \tag{3a, b}$$

where the symbolic form $\mathbf{u}[\ldots]$ and $\mathbf{t}[\ldots]$ has been used for simplicity. For a more detailed description of these equations, the reader can refer to Panzeca et al. [4].

In Eqs. (3a, b) the typologies of the boundary are characterized by the subscripts introduced in the displacement and traction vectors. The apices CPV, present in the terms $\mathbf{u}_1\ [-\mathbf{u}_1^{CPV}]$ and $\mathbf{t}_2\ [\mathbf{f}_2^{CPV}]$, mean that the related integrals have to be considered as the Cauchy Principal Value, whereas the coefficients where $1/2$ occurs are the free terms shown in explicit form.

To analyze the contact-detachment problem, it is necessary to define the unknowns $\mathbf{u}_{0v}$ and $\mathbf{t}_{0v}$, related to the virtual boundary Γ_{0v}

$$\begin{aligned} \mathbf{u}_{0v} &= \mathbf{u}_{0v}\left[\mathbf{f}_1, -\mathbf{u}_2, \mathbf{f}_{0v}, -\mathbf{u}_{0v}^{CPV}, \mathbf{f}_{0r}, -\mathbf{u}_{0r}\right] \\ &\quad + \frac{1}{2}\mathbf{u}_{0v} + \underbrace{\mathbf{u}_{0v}\left[\bar{\mathbf{f}}_2, -\bar{\mathbf{u}}_1, \bar{\mathbf{b}}\right]}_{\hat{\mathbf{u}}_{0v}} \\ \mathbf{t}_{0v} &= \mathbf{t}_{0v}\left[\mathbf{f}_1, -\mathbf{u}_2, \mathbf{f}_{0v}^{CPV}, -\mathbf{u}_{0v}, \mathbf{f}_{0r}, -\mathbf{u}_{0r}\right] \\ &\quad + \frac{1}{2}\mathbf{t}_{0v} + \underbrace{\mathbf{t}_{0v}\left[\bar{\mathbf{f}}_2, -\bar{\mathbf{u}}_1, \bar{\mathbf{b}}\right]}_{\hat{\mathbf{t}}_{0v}} \end{aligned} \tag{4a, b}$$

and the unknowns $\mathbf{u}_{0r}$ and $\mathbf{t}_{0r}$, related to the real boundary Γ_{0r}

$$\begin{aligned} \mathbf{u}_{0r} &= \mathbf{u}_{0r}\left[\mathbf{f}_1, -\mathbf{u}_2, \mathbf{f}_{0v}, -\mathbf{u}_{0v}, \mathbf{f}_{0r}, -\mathbf{u}_{0r}^{CPV}\right] \\ &\quad + \frac{1}{2}\mathbf{u}_{0r} + \underbrace{\mathbf{u}_{0r}\left[\bar{\mathbf{f}}_2, -\bar{\mathbf{u}}_1, \bar{\mathbf{b}}\right]}_{\hat{\mathbf{u}}_{0r}} \\ \mathbf{t}_{0r} &= \mathbf{t}_{0r}\left[\mathbf{f}_1, -\mathbf{u}_2, \mathbf{f}_{0v}, -\mathbf{u}_{0v}, \mathbf{f}_{0r}^{CPV}, -\mathbf{u}_{0r}\right] \\ &\quad + \frac{1}{2}\mathbf{t}_{0r} + \underbrace{\mathbf{t}_{0r}\left[\bar{\mathbf{f}}_2, -\bar{\mathbf{u}}_1, \bar{\mathbf{b}}\right]}_{\hat{\mathbf{t}}_{0r}} \end{aligned} \tag{5a, b}$$

Author's personal copy

Eqs. (3a, b) can be rewritten in a different way

$$\begin{aligned}
&\mathbf{u}_1\,[\mathbf{f}_1,-\mathbf{u}_2,\mathbf{f}_{0v},-\mathbf{u}_{0v},\mathbf{f}_{0r},-\mathbf{u}_{0r}]\\
&\quad+\underbrace{\mathbf{u}_1\left[\bar{\mathbf{f}}_2,-\bar{\mathbf{u}}_1^{CPV},\bar{\mathbf{b}}\right]-\frac{1}{2}\bar{\mathbf{u}}_1}_{\hat{\mathbf{u}}_1}=\mathbf{0}\\
&\mathbf{t}_2\,[\mathbf{f}_1,-\mathbf{u}_2,\mathbf{f}_{0v},-\mathbf{u}_{0v},\mathbf{f}_{0r},-\mathbf{u}_{0r}]\\
&\quad+\underbrace{\mathbf{t}_2\left[\bar{\mathbf{f}}_2^{CPV},-\bar{\mathbf{u}}_1,\bar{\mathbf{b}}\right]-\frac{1}{2}\bar{\mathbf{f}}_2}_{\hat{\mathbf{t}}_2}=\mathbf{0}
\end{aligned}\qquad(6a,\,b)$$

whereas Eqs. (4a, b) and Eqs. (5a, b) remain unchanged.

We introduce the boundary discretization into boundary elements and perform the following modelling of all the known and unknown quantities:

$$\begin{aligned}
&\mathbf{f}_1=\boldsymbol{\Psi}_f\,\mathbf{F}_1,\ \bar{\mathbf{f}}_2=\boldsymbol{\Psi}_f\,\bar{\mathbf{F}}_2,\ \mathbf{t}_{0v}=\boldsymbol{\Psi}_f\,\mathbf{F}_{0v},\ \mathbf{t}_{0r}=\boldsymbol{\Psi}_f\,\mathbf{F}_{0r},\\
&\bar{\mathbf{u}}_1=\boldsymbol{\Psi}_u\,\bar{\mathbf{U}}_1,\ \ \mathbf{u}_2=\boldsymbol{\Psi}_u\,\mathbf{U}_2,\ \mathbf{u}_{0v}=\boldsymbol{\Psi}_u\,\mathbf{U}_{0v},\ \mathbf{u}_{0r}=\boldsymbol{\Psi}_u\,\mathbf{U}_{0r}
\end{aligned}\qquad(7a\text{–}h)$$

where $\boldsymbol{\Psi}_t$ and $\boldsymbol{\Psi}_u$ are appropriate matrices of linear shape functions modelling the boundary quantities. Further, the capital letters indicate the nodal vectors of the forces ($\mathbf{F}_1$, $\bar{\mathbf{F}}_2$, $\mathbf{F}_{0v}$ and $\mathbf{F}_{0r}$) and of the displacements ($\bar{\mathbf{U}}_1$, $\mathbf{U}_2$, $\mathbf{U}_{0v}$ and $\mathbf{U}_{0r}$) defined at the boundary nodes.

We now perform the weighting of all the coefficients of Eqs. (4–6). For this purpose, the same shape functions as those modelling the causes (see Eqs. (7a–h)) are employed, but introduced in an energetically dual way according to the Galerkin approach [24], thus obtaining the following equations whose coefficients symbolize generalized quantities:

$$\begin{aligned}
&\mathbf{W}_1=\int_{\Gamma_1}\boldsymbol{\Psi}_f^T\mathbf{u}_1,\qquad \mathbf{P}_2=\int_{\Gamma_2}\boldsymbol{\Psi}_u^T\,\mathbf{t}_2,\\
&\mathbf{W}_{0v}=\int_{\Gamma_{0v}}\boldsymbol{\Psi}_f^T\mathbf{u}_{0v},\quad \mathbf{P}_{0v}=\int_{\Gamma_{0v}}\boldsymbol{\Psi}_u^T\,\mathbf{t}_{0v},\\
&\mathbf{W}_{0r}=\int_{\Gamma_{0r}}\boldsymbol{\Psi}_f^T\mathbf{u}_{0r},\quad \mathbf{P}_{0r}=\int_{\Gamma_{0r}}\boldsymbol{\Psi}_u^T\,\mathbf{t}_{0r}
\end{aligned}\qquad(8a\text{–}f)$$

As a consequence, these equations are rewritten in the following symbolic form:

$$\begin{aligned}
&\mathbf{W}_1\,[\mathbf{F}_1,-\mathbf{U}_2,\mathbf{F}_{0v},-\mathbf{U}_{0v},\mathbf{F}_{0r},-\mathbf{U}_{0r}]+\hat{\mathbf{W}}_1=\mathbf{0}\\
&\mathbf{P}_2\,[\mathbf{F}_1,-\mathbf{U}_2,\mathbf{F}_{0v},-\mathbf{U}_{0v},\mathbf{F}_{0r},-\mathbf{U}_{0r}]+\hat{\mathbf{P}}_2=\mathbf{0}\\
&\mathbf{W}_{0v}=\mathbf{W}_{0v}\,[\mathbf{F}_1,-\mathbf{U}_2,\mathbf{F}_{0v},-\mathbf{U}_{0v},\mathbf{F}_{0r},-\mathbf{U}_{0r}]+\hat{\mathbf{W}}_{0v}\\
&\mathbf{P}_{0v}=\mathbf{P}_{0v}\,[\mathbf{F}_1,-\mathbf{U}_2,\mathbf{F}_{0v},-\mathbf{U}_{0v},\mathbf{F}_{0r},-\mathbf{U}_{0r}]+\hat{\mathbf{P}}_{0v}\\
&\mathbf{W}_{0r}=\mathbf{W}_{0r}\,[\mathbf{F}_1,-\mathbf{U}_2,\mathbf{F}_{0v},-\mathbf{U}_{0v},\mathbf{F}_{0r},-\mathbf{U}_{0r}]+\hat{\mathbf{W}}_{0r}\\
&\mathbf{P}_{0r}=\mathbf{P}_{0r}\,[\mathbf{F}_1,-\mathbf{U}_2,\mathbf{F}_{0v},-\mathbf{U}_{0v},\mathbf{F}_{0r},-\mathbf{U}_{0r}]+\hat{\mathbf{P}}_{0r}
\end{aligned}\qquad(9a\text{–}f)$$

or in the following equivalent block system:

$$\begin{vmatrix}\mathbf{0}\\ \mathbf{0}\\ \mathbf{W}_{0v}\\ \mathbf{P}_{0v}\\ \mathbf{W}_{0r}\\ \mathbf{P}_{0r}\end{vmatrix}=\begin{vmatrix}\mathbf{A}_{u1u1}&\mathbf{A}_{u1f2}&\mathbf{A}_{u1uv}&\mathbf{A}_{u1fv}&\mathbf{A}_{u1ur}&\mathbf{A}_{u1fr}\\ \mathbf{A}_{f2u1}&\mathbf{A}_{f2f2}&\mathbf{A}_{f2uv}&\mathbf{A}_{f2fv}&\mathbf{A}_{f2ur}&\mathbf{A}_{f2fr}\\ \mathbf{A}_{uvu1}&\mathbf{A}_{uvf2}&\mathbf{A}_{uvuv}&\overline{\mathbf{A}}_{uvfv}&\mathbf{A}_{uvur}&\mathbf{A}_{uvfr}\\ \mathbf{A}_{fvu1}&\mathbf{A}_{fvf2}&\overline{\mathbf{A}}_{fvuv}&\mathbf{A}_{fvfv}&\mathbf{A}_{fvur}&\mathbf{A}_{fvfr}\\ \mathbf{A}_{uru1}&\mathbf{A}_{urf2}&\mathbf{A}_{uruv}&\mathbf{A}_{urfv}&\mathbf{A}_{urur}&\overline{\mathbf{A}}_{urfr}\\ \mathbf{A}_{fru1}&\mathbf{A}_{frf2}&\mathbf{A}_{fruv}&\mathbf{A}_{frfv}&\overline{\mathbf{A}}_{frur}&\mathbf{A}_{frfr}\end{vmatrix}\begin{vmatrix}\mathbf{F}_1\\ -\mathbf{U}_2\\ \mathbf{F}_{0v}\\ -\mathbf{U}_{0v}\\ \mathbf{F}_{0r}\\ -\mathbf{U}_{0r}\end{vmatrix}+\begin{vmatrix}\hat{\mathbf{W}}_1\\ \hat{\mathbf{P}}_2\\ \hat{\mathbf{W}}_{0v}\\ \hat{\mathbf{P}}_{0v}\\ \hat{\mathbf{W}}_{0r}\\ \hat{\mathbf{P}}_{0r}\end{vmatrix}\qquad(10)$$

where the load terms are the following:

$$\begin{aligned}
&\hat{\mathbf{W}}_1=\int_{\Gamma_1}\boldsymbol{\psi}_f^T\,\hat{\mathbf{u}}_1=\int_{\Gamma_1}\boldsymbol{\psi}_f^T\left(\mathbf{u}_1\left[\bar{\mathbf{f}}_2,-\bar{\mathbf{u}}_1^{CPV},\bar{\mathbf{b}}\right]-\frac{1}{2}\bar{\mathbf{u}}_1\right)\\
&\hat{\mathbf{P}}_2=\int_{\Gamma_2}\boldsymbol{\psi}_u^T\,\hat{\mathbf{f}}_2=\int_{\Gamma_2}\boldsymbol{\psi}_u^T\left(\mathbf{t}_2\left[\bar{\mathbf{f}}_2^{\mathrm{CPV}},-\bar{\mathbf{u}}_1,\bar{\mathbf{b}}\right]-\frac{1}{2}\bar{\mathbf{f}}_2\right)\\
&\hat{\mathbf{W}}_{0v}=\int_{\Gamma_{0v}}\boldsymbol{\psi}_f^T\,\hat{\mathbf{u}}_{0v}=\int_{\Gamma_{0v}}\boldsymbol{\psi}_f^T\,\mathbf{u}_{0v}\left[\bar{\mathbf{f}}_2,-\bar{\mathbf{u}}_1,\bar{\mathbf{b}}\right]\\
&\hat{\mathbf{P}}_{0v}=\int_{\Gamma_{0v}}\boldsymbol{\psi}_u^T\,\hat{\mathbf{t}}_{0v}=\int_{\Gamma_{0v}}\boldsymbol{\psi}_u^T\,\mathbf{t}_{0v}\left[\bar{\mathbf{f}}_2,-\bar{\mathbf{u}}_1,\bar{\mathbf{b}}\right]\\
&\hat{\mathbf{W}}_{0r}=\int_{\Gamma_{0r}}\boldsymbol{\psi}_f^T\,\hat{\mathbf{u}}_{0r}=\int_{\Gamma_{0r}}\boldsymbol{\psi}_f^T\,\mathbf{u}_{0r}\left[\bar{\mathbf{f}}_2,-\bar{\mathbf{u}}_1,\bar{\mathbf{b}}\right]\\
&\hat{\mathbf{P}}_{0r}=\int_{\Gamma_{0r}}\boldsymbol{\psi}_u^T\,\hat{\mathbf{t}}_{0r}=\int_{\Gamma_{0r}}\boldsymbol{\psi}_u^T\,\mathbf{t}_{0r}\left[\bar{\mathbf{f}}_2,-\bar{\mathbf{u}}_1,\bar{\mathbf{b}}\right]
\end{aligned}\qquad(10a,\,f)$$

It is to be noted that in the latter block equation the matrix $\mathbf{A}$, where the subscripts 0 have been omitted for simplicity, is symmetric. Moreover, the submatrices and the load subvectors $\hat{\mathbf{W}}$, $\hat{\mathbf{P}}$ are made by coefficients obtained through a double integration according to the SGBEM strategy. In detail, the first and second rows represent the Dirichlet and Neumann conditions (Eqs. 2a, b) written in weighted form $\mathbf{W}_1-\overline{\mathbf{W}}_1=\mathbf{0}$ on Γ_1 and $\mathbf{P}_2-\overline{\mathbf{P}}_2=\mathbf{0}$ on Γ_2. The remaining rows regard the weighting of the displacements and tractions in the real and virtual contact zones defined on the boundary $\Gamma_0=\Gamma_{0r}\cup\Gamma_{0v}$. The terms $\overline{\mathbf{A}}_{\mathrm{urfr}}=\overline{\mathbf{A}}_{\mathrm{frur}}^T$ and $\overline{\mathbf{A}}_{\mathrm{uvfv}}=\overline{\mathbf{A}}_{\mathrm{fvuv}}^T$ include the weighting of the CPV integrals and of the related free terms.

In Eq. (10) some coefficients show singular or hypersingular kernels. These difficulties were overcome within the SGBEM approach by using different techniques. The reader can refer to Terravecchia [25] for a more detailed discussion of the computational aspects and for the related references.

Author's personal copy

Eq. (10) can be expressed in compact form in the following way:

$$\mathbf{0} = \mathbf{A}\,\mathbf{X} + \mathbf{A}_0\mathbf{X}_0 + \hat{\mathbf{L}}$$
$$\mathbf{Z}_0 = \mathbf{A}_0^T\mathbf{X} + \mathbf{A}_{00}\mathbf{X}_0 + \hat{\mathbf{L}}_0 \qquad (11a, b)$$

where the following positions are set

$$\mathbf{Z}_0 = \begin{vmatrix} \mathbf{W}_{0v} \\ \mathbf{P}_{0v} \\ \mathbf{W}_{0r} \\ \mathbf{P}_{0r} \end{vmatrix}, \quad \mathbf{X} = \begin{vmatrix} \mathbf{F}_1 \\ -\mathbf{U}_2 \end{vmatrix}, \quad \mathbf{X}_0 = \begin{vmatrix} \mathbf{F}_{0v} \\ -\mathbf{U}_{0v} \\ \mathbf{F}_{0r} \\ -\mathbf{U}_{0r} \end{vmatrix},$$

$$\hat{\mathbf{L}} = \begin{vmatrix} \hat{\mathbf{W}}_1 \\ \hat{\mathbf{P}}_2 \end{vmatrix}, \quad \hat{\mathbf{L}}_0 = \begin{vmatrix} \hat{\mathbf{W}}_{0v} \\ \hat{\mathbf{P}}_{0v} \\ \hat{\mathbf{W}}_{0r} \\ \hat{\mathbf{P}}_{0r} \end{vmatrix} \qquad (12a–e)$$

The vector $\mathbf{Z}_0$ collects the generalized (or weighted) displacement $\mathbf{W}_0$ and traction $\mathbf{P}_0$ subvectors defined at the real and virtual boundaries, obtained as the response to all the known and unknown actions, regarding the boundary and domain quantities. By performing variable condensation through the replacement of the vector $\mathbf{X}$ extracted from Eq. (11a) into Eq. (11b), one obtains:

$$\mathbf{Z}_0 = \mathbf{D}_{00}\,\mathbf{X}_0 + \overline{\mathbf{Z}}_0 \qquad (13a)$$

or in extensive form

$$\begin{vmatrix} \mathbf{W}_{0v} \\ \mathbf{P}_{0v} \\ \mathbf{W}_{0r} \\ \mathbf{P}_{0r} \end{vmatrix} = \begin{vmatrix} \mathbf{D}_{uvuv} & \mathbf{D}_{uvfv} & \mathbf{D}_{uvur} & \mathbf{D}_{uvfr} \\ \mathbf{D}_{fvuv} & \mathbf{D}_{fvfv} & \mathbf{D}_{fvur} & \mathbf{D}_{fvfr} \\ \mathbf{D}_{uruv} & \mathbf{D}_{urfv} & \mathbf{D}_{urur} & \mathbf{D}_{urfr} \\ \mathbf{D}_{fruv} & \mathbf{D}_{frfv} & \mathbf{D}_{frur} & \mathbf{D}_{frfr} \end{vmatrix} \begin{vmatrix} \mathbf{F}_0 v \\ -\mathbf{U}_{0v} \\ \mathbf{F}_{0r} \\ -\mathbf{U}_{0r} \end{vmatrix} + \begin{vmatrix} \overline{\mathbf{W}}_{0v} \\ \overline{\mathbf{P}}_{0v} \\ \overline{\mathbf{W}}_{0r} \\ \overline{\mathbf{P}}_{0r} \end{vmatrix} \qquad (13b)$$

In Eq. (13a), one has set

$$\mathbf{D}_{00} = \mathbf{A}_0^T\,\mathbf{A}^{-1}\,\mathbf{A}_0 - \mathbf{A}_{00},\ \overline{\mathbf{Z}}_0 = -\mathbf{A}_0^T\,\mathbf{A}^{-1}\,\hat{\mathbf{L}} + \hat{\mathbf{L}}_0 \qquad (14a, b)$$

Eq. (13a) is the elastic equation written for each of two BEM-elements. It relates the generalized (or weighted) displacement and traction vectors, collected in $\mathbf{Z}_0$ at the real and virtual boundary Γ_0, to the force and displacement nodal vector $\mathbf{X}_0$ of the same boundary and to the load vector $\overline{\mathbf{Z}}_0$. Moreover, $\mathbf{D}_{00}$ is an appropriate pseudo-stiffness matrix of the BEM-e being examined.

2.2 BEM-element assembly

We want to obtain an equation system able to give an elastic solution for an assigned configuration during a loading process which for two bodies in contact contemplates the possibility of modifying the contact zone. The strategy is based on the approach of multi-connected bodies handled using the symmetric BEM. For each BEM-e, equations like Eq. (13) can be written, i.e.:

$$\mathbf{Z}_0^A = \mathbf{D}_{00}^A\,\mathbf{X}_0^A + \overline{\mathbf{Z}}_0^A \quad \text{for body } A \qquad (15a)$$
$$\mathbf{Z}_0^B = \mathbf{D}_{00}^B\,\mathbf{X}_0^B + \overline{\mathbf{Z}}_0^B \quad \text{for body } B \qquad (15b)$$

Now we impose the regularity conditions (or coupling conditions) between the BEM-elements in order to guarantee the kinematical and mechanical regularity conditions both in terms of nodal variables (strong regularity) and in terms of generalized quantities (weak regularity) at the nodes of the real interface zone Γ_{0r}, i.e.:

$$\mathbf{W}_{0r}^A = \mathbf{W}_{0r}^B \quad \text{weak compatibility on } \Gamma_{0r} \qquad (16a)$$
$$\mathbf{P}_{0r}^A = -\mathbf{P}_{0r}^B \quad \text{weak equilibrium on } \Gamma_{0r} \qquad (16b)$$

$$\mathbf{U}_{0r}^A = \mathbf{U}_{0r}^B = \mathbf{U}_{0r} \quad \text{strong compatibility on } \Gamma_{0r} \qquad (17a)$$
$$\mathbf{F}_{0r}^A = -\mathbf{F}_{0r}^B = \mathbf{F}_{0r} \quad \text{strong equilibrium on } \Gamma_{0r} \qquad (17b)$$

Moreover, Γ_{0v} being a Neumann type boundary, we can write:

$$\mathbf{P}_{0v}^A = \mathbf{P}_{0v}^B = \mathbf{0}\,,\quad \mathbf{F}_{0v}^A = \mathbf{F}_{0v}^B = \mathbf{0} \qquad \text{on } \Gamma_{0v} \qquad (18a, b)$$

Eqs. (15–17) give rise to the following block system:

$$\begin{vmatrix} \mathbf{W}_{0v}^A \\ \mathbf{W}_{0v}^B \\ \mathbf{P}_{0v}^A = \mathbf{0} \\ \mathbf{P}_{0v}^B = \mathbf{0} \\ \mathbf{W}_{0r}^A - \mathbf{W}_{0r}^B = \mathbf{0} \\ \mathbf{P}_{0r}^A + \mathbf{P}_{0r}^B = \mathbf{0} \end{vmatrix} = \begin{vmatrix} \mathbf{D}_{uvfv}^A & \mathbf{0} & \mathbf{D}_{uvur}^A & \mathbf{D}_{uvfr}^A \\ \mathbf{0} & \mathbf{D}_{uvfv}^B & -\mathbf{D}_{uvur}^B & \mathbf{D}_{uvfr}^B \\ \mathbf{D}_{fvfv}^A & \mathbf{0} & \mathbf{D}_{fvur}^A & \mathbf{D}_{fvfr}^A \\ \mathbf{0} & \mathbf{D}_{fvfv}^B & -\mathbf{D}_{fvur}^B & \mathbf{D}_{fvfr}^B \\ \mathbf{D}_{urfv}^A & -\mathbf{D}_{urfv}^B & \left(\mathbf{D}_{urur}^A + \mathbf{D}_{urur}^B\right) & \left(\mathbf{D}_{urfr}^A - \mathbf{D}_{urfr}^B\right) \\ \mathbf{D}_{frfv}^A & \mathbf{D}_{frfv}^B & \left(\mathbf{D}_{frur}^A - \mathbf{D}_{frur}^B\right) & \left(\mathbf{D}_{frfr}^A + \mathbf{D}_{frfr}^B\right) \end{vmatrix} \begin{vmatrix} -\mathbf{U}_{0v}^A \\ -\mathbf{U}_{0v}^B \\ \mathbf{F}_{0r} \\ -\mathbf{U}_{0r} \end{vmatrix} + \begin{vmatrix} \overline{\mathbf{W}}_{0v}^A \\ \overline{\mathbf{W}}_{0v}^B \\ \overline{\mathbf{P}}_{0v}^A \\ \overline{\mathbf{P}}_{0v}^B \\ \left(\overline{\mathbf{W}}_{0r}^A - \overline{\mathbf{W}}_{0r}^B\right) \\ \left(\overline{\mathbf{P}}_{0r}^A + \overline{\mathbf{P}}_{0r}^B\right) \end{vmatrix} \qquad (19)$$

In this block system, the first four rows regard the virtual boundary Γ_{0v} and represent the response in terms of weighted displacements and weighted tractions (the latter null by definition) related to two bodies A and B in contact. The fifth and sixth rows represent the weighted regularity conditions related to the real boundary Γ_{0r}, that is to say they are the expressions characterizing the weak compatibility of the displacements and the weak equilibrium of the tractions satisfying conditions (16a, b).

Eq. (19) is now reduced by removing the first and the second block rows regarding the weighted displacements

Author's personal copy

$\mathbf{W}^A_{0v}$, $\mathbf{W}^B_{0v}$ on the boundary Γ_{0v}, thus obtaining the following block equation:

$$\begin{vmatrix} \mathbf{D}^A_{fvfv} & \mathbf{0} & \mathbf{D}^A_{fvur} & \mathbf{D}^A_{fvfr} \\ \mathbf{0} & \mathbf{D}^B_{fvfv} & -\mathbf{D}^B_{fvur} & \mathbf{D}^B_{fvfr} \\ \mathbf{D}^A_{urfv} & -\mathbf{D}^B_{urfv} & \left(\mathbf{D}^A_{urur}+\mathbf{D}^B_{urur}\right) & \left(\mathbf{D}^A_{urfr}-\mathbf{D}^B_{urfr}\right) \\ \mathbf{D}^A_{frfv} & \mathbf{D}^B_{frfv} & \left(\mathbf{D}^A_{frur}-\mathbf{D}^B_{frur}\right) & \left(\mathbf{D}^A_{frfr}+\mathbf{D}^B_{frfr}\right) \end{vmatrix} \begin{vmatrix} -\mathbf{U}^A_{0v} \\ -\mathbf{U}^B_{0v} \\ \mathbf{F}_{0r} \\ -\mathbf{U}_{0r} \end{vmatrix} + \begin{vmatrix} \overline{\mathbf{P}}^A_{0v} \\ \overline{\mathbf{P}}^B_{0v} \\ \left(\overline{\mathbf{W}}^A_{0r}-\overline{\mathbf{W}}^B_{0r}\right) \\ \left(\overline{\mathbf{P}}^A_{0r}+\overline{\mathbf{P}}^B_{0r}\right) \end{vmatrix} = \begin{vmatrix} \mathbf{0} \\ \mathbf{0} \\ \mathbf{0} \\ \mathbf{0} \end{vmatrix} \tag{20}$$

The two block rows $\mathbf{W}^A_{0v}$ and $\mathbf{W}^B_{0v}$ of the system (19) have been used for the solution of the contact-detachment problem through iterative LCP with the use of generalized variables as described by Panzeca et al. in [5].

Eq. (20) can be expressed in compact form in the following way:

$$\begin{aligned} &\mathbf{H}_{tt}\,\mathbf{Y}_0 + \mathbf{H}_{tr}\,(-\mathbf{U}_{0r}) + \overline{\mathbf{G}}_t = \mathbf{0} \\ &\mathbf{H}_{rt}\,\mathbf{Y}_0 + \mathbf{H}_{rr}\,(-\mathbf{U}_{0r}) + \overline{\mathbf{G}}_r = \mathbf{0} \end{aligned} \tag{21a,b}$$

where the index $t = 2v + r$, with v the node number of the virtual boundary Γ_{0v} and r the node number of the real boundary Γ_{0r}.

The following positions were set for the vectors

$$\mathbf{Y}_0 = \begin{vmatrix} -\mathbf{U}^A_{0v} \\ -\mathbf{U}^B_{0v} \\ \mathbf{F}_{0r} \end{vmatrix}, \overline{\mathbf{G}}_t = \begin{vmatrix} \overline{\mathbf{P}}^A_{0v} \\ \overline{\mathbf{P}}^B_{0v} \\ \left(\overline{\mathbf{W}}^A_{0r}-\overline{\mathbf{W}}^B_{0r}\right) \end{vmatrix}, \quad \overline{\mathbf{G}}_r = \left| \left(\overline{\mathbf{P}}^A_{0r}+\overline{\mathbf{P}}^A_{0r}\right) \right| \tag{22a–c}$$

and for the matrices

$$\mathbf{H}_{tt} = \begin{vmatrix} \mathbf{D}^A_{fvfv} & \mathbf{0} & \mathbf{D}^A_{fvur} \\ \mathbf{0} & \mathbf{D}^B_{fvfv} & -\mathbf{D}^B_{fvur} \\ \mathbf{D}^A_{urfv} & -\mathbf{D}^B_{urfv} & \left(\mathbf{D}^A_{urur}+\mathbf{D}^B_{urur}\right) \end{vmatrix}, \quad \mathbf{H}_{tr} = \mathbf{H}^T_{rt} = \begin{vmatrix} \mathbf{D}^A_{fvfr} \\ \mathbf{D}^B_{fvfr} \\ \left(\mathbf{D}^A_{urfr}-\mathbf{D}^B_{urfr}\right) \end{vmatrix}, \quad \mathbf{H}_{rr} = \left| \left(\mathbf{D}^A_{frfr}+\mathbf{D}^B_{frfr}\right) \right| \tag{22d–f}$$

By performing a variable condensation through the replacement of the vector $(-\mathbf{U}_{0r})$ extracted from Eq. (21b) into Eq. (21a), one obtains:

$$\begin{vmatrix} \mathbf{K}^{AA}_{fvfv} & \mathbf{K}^{AB}_{fvfv} & \mathbf{K}^{A}_{fvur} \\ \mathbf{K}^{BA}_{fvfv} & \mathbf{K}^{BB}_{fvfv} & \mathbf{K}^{B}_{fvur} \\ \mathbf{K}^{A}_{urfv} & \mathbf{K}^{B}_{urfv} & \mathbf{K}_{urur} \end{vmatrix} \begin{vmatrix} -\mathbf{U}^A_{0v} \\ -\mathbf{U}^B_{0v} \\ \mathbf{F}_{0r} \end{vmatrix} + \begin{vmatrix} \overline{\mathbf{L}}^A_{fv} \\ \overline{\mathbf{L}}^B_{fv} \\ \overline{\mathbf{L}}_{ur} \end{vmatrix} = \begin{vmatrix} \mathbf{0} \\ \mathbf{0} \\ \mathbf{0} \end{vmatrix}$$

$$\text{i.e. } \mathbf{K}_{00}\,\mathbf{Y}_0 + \overline{\mathbf{L}}_0 = \mathbf{0} \tag{23}$$

with

$$\mathbf{K}_{00} = \mathbf{H}_{tt} - \mathbf{H}_{tr}\mathbf{H}^{-1}_{rr}\mathbf{H}_{rt},\ \overline{\mathbf{L}}_0 = \overline{\mathbf{G}}_t - \mathbf{H}_{tr}\mathbf{H}^{-1}_{rr}\overline{\mathbf{G}}_r \tag{24a, b}$$

The sub-matrices of $\mathbf{K}_{00}$ show double indices, the first characterizing the weighted quantities $\mathbf{P}$ along the virtual boundaries of A and B and $\mathbf{W}$ along the real one, and the second the nodal quantity associated with the node in dual form on the same boundaries, considered as causes.

In order to distinguish the variables related to the virtual and real boundaries, equation (23) can be written in a more compact form:

$$\begin{vmatrix} \mathbf{K}_{fvfv} & \mathbf{K}_{fvur} \\ \mathbf{K}_{urfv} & \mathbf{K}_{urur} \end{vmatrix} \begin{vmatrix} -\mathbf{U}_{0v} \\ \mathbf{F}_{0r} \end{vmatrix} + \begin{vmatrix} \overline{\mathbf{L}}_{fv} \\ \overline{\mathbf{L}}_{ur} \end{vmatrix} = \begin{vmatrix} \mathbf{0} \\ \mathbf{0} \end{vmatrix}$$

$$\text{i.e. } \mathbf{K}_{00}\,\mathbf{Y}_0 + \overline{\mathbf{L}}_0 = \mathbf{0} \tag{25}$$

where the subvectors $(-\mathbf{U}_{0v}) = \left[\left(-\mathbf{U}^A_{0v}\right)^T \quad \left(-\mathbf{U}^B_{0v}\right)^T\right]^T$ and $\overline{\mathbf{L}}_{fv} = \left[\left(\overline{\mathbf{L}}^A_{fv}\right)^T \quad \left(\overline{\mathbf{L}}^B_{fv}\right)^T\right]^T$ have been introduced and where the submatrices assume an obvious meaning.

The four sub-matrices that define the matrix $\mathbf{K}_{00}$ have the following meaning:

- The submatrix $\mathbf{K}_{fvfv}$ relates the weighted tractions $\mathbf{P}_{0v}$ on the virtual boundary elements Γ_{0v} of the two bodies A and B to the nodal displacements $(-\mathbf{U}_{0v})$ of the same boundaries. This matrix is symmetric and negative definite; it takes on the meaning of a stiffness matrix.
- The submatrix $\mathbf{K}_{fvur}$ relates the weighted tractions $\mathbf{P}_{0v}$ on the virtual boundary elements Γ_{0v} of the two bodies A and B to the nodal forces $\mathbf{F}_{0r}$ of the real boundary Γ_{0r}. This matrix takes on the meaning of an equilibrium matrix.
- The submatrix $\mathbf{K}_{urfv}$ relates the weighted displacements $\mathbf{W}_{0r}$ on the real boundary elements Γ_{0r} to the nodal diplacements $(-\mathbf{U}_{0v})$ of the virtual boundary Γ_{0v}. This matrix therefore takes on the meaning of a compatibility matrix.
- The submatrix $\mathbf{K}_{urur}$ relates the weighted displacements $\mathbf{W}_{0r}$ on the real boundary elements Γ_{0r} to the nodal forces $\mathbf{F}_{0r}$ of the same boundary. This matrix is symmetric and positive definite; it therefore takes on the meaning of a flexibility matrix.

The load vector $\overline{\mathbf{L}}_0$ collects the response in terms of weighted mechanical and kinematical quantities to all the external actions i.e.:

Author's personal copy

– the sub-vector $\overline{\mathbf{L}}_{fv}$ collects the weighted tractions on the virtual boundary elements Γ_{0v} given by all the known mechanical and kinematical actions of the assembling system.
– the sub-vector $\overline{\mathbf{L}}_{ur}$ collects the weighted displacements on the real boundary elements Γ_{0r} given by all the known mechanical and kinematical actions.

By performing a diagonalization process of Eq. (25), one obtains

$$\begin{vmatrix} \tilde{\mathbf{K}}_{fvfv} & \mathbf{0} \\ \mathbf{0} & \tilde{\mathbf{K}}_{urur} \end{vmatrix} \begin{vmatrix} -\mathbf{U}_{0v} \\ \mathbf{F}_{0r} \end{vmatrix} + \begin{vmatrix} \tilde{\mathbf{L}}_{fv} \\ \tilde{\mathbf{L}}_{ur} \end{vmatrix} = \begin{vmatrix} \mathbf{0} \\ \mathbf{0} \end{vmatrix}$$
$$i.e.\ \tilde{\mathbf{K}}_{00}\mathbf{Y}_0 + \tilde{\mathbf{L}}_0 = \mathbf{0} \tag{26}$$

where one has set

$$\begin{aligned} \tilde{\mathbf{K}}_{urur} &= \mathbf{K}_{urur} - \mathbf{K}_{urfv}\left(\mathbf{K}_{fvfv}\right)^{-1}\mathbf{K}_{fvur}, \\ \tilde{\mathbf{L}}_{ur} &= \overline{\mathbf{L}}_{ur} - \mathbf{K}_{urfv}\left(\mathbf{K}_{fvfv}\right)^{-1}\overline{\mathbf{L}}_{fv}, \\ \tilde{\mathbf{K}}_{fvfv} &= \mathbf{K}_{fvfv} - \mathbf{K}_{fvur}\left(\mathbf{K}_{urur}\right)^{-1}\mathbf{K}_{urfv}, \\ \tilde{\mathbf{L}}_{fv} &= \overline{\mathbf{L}}_{fv} - \mathbf{K}_{fvur}\left(\mathbf{K}_{urur}\right)^{-1}\overline{\mathbf{L}}_{ur}. \end{aligned} \tag{27}$$

The two equations extracted from Eq. (26) $\tilde{\mathbf{K}}_{fvfv}(-\mathbf{U}_{0v}) + \tilde{\mathbf{L}}_{fv} = \mathbf{0}$ and $\tilde{\mathbf{K}}_{urur}\mathbf{F}_{0r} + \tilde{\mathbf{L}}_{ur} = \mathbf{0}$ give the displacements of the virtual boundary and the forces of the real one, respectively, both based on the mixed variable approach of the multidomain SGBEM. These equations can be used to obtain the solution in a contact-detachment process through the LCP, following an iterative procedure, or solving a *min-max* problem of an appropriate functional through the QPP.

The algebraic operators in Eq. (25), or alternatively in Eq. (26) obtained by Eq. (10), are the basis of the two strategies that will be shown in the following sections and involve high computational advantages in the solution of the contact-detachment problem. Indeed:

– in the LCP strategy, when a part the real interface boundary Γ_{0r} changes into a virtual interface boundary Γ_{0v} (detachment) or, vice versa, when a part of the boundary Γ_{0v} changes into a boundary Γ_{0r} (contact), the operator dimensions do not change, but some blocks of rows and columns simply exchange their collocation without the need to be re-computed;
– in the QPP strategy, the same operators are used because they take on an essential role in defining the nonlinear problem.

The flexibility of the algebraic operators gives high performance to the proposed methodologies in order to reduce the computational burdens.

3 The contact-detachment problem

Once all the operators governing the elastic analysis phase based on the multidomain SGBEM approach have been determined, it is possible to define the strategies that allow us to get the solution to the contact-detachment problem. In detail two alternative strategies are shown:

– The first strategy, shown in Sect. 3.1, is an analysis in which the solution to the contact-detachment problem is obtained iteratively as the solution to a LCP approach. This is made possible by coupling the elastic solution given in Eq. (25) with the contact-detachment conditions introduced by Signorini [1], rewritten in terms of nodal quantities. This strategy proves to be onerous from the computational point of view but has high performance, since it is able to give a lot of information during the contact-detachment process.
– The second strategy shown in Sect. 3.2 is an analysis based on the solution to a *min-max* problem of a reduced functional whose solution is obtained through the QPP approach. This *min-max* problem may be de-coupled into two independent sub-problems of *min* and *max*, able to analyse the contact and detachment separately, thus reducing the computational burdens of the quadratic programming. The solution to this problem is very advantageous in terms of CPU times, but it shows loss of consistency since it is unable to give information regarding, for instance, the stress and strain states during the contact-detachment process.

Both these strategies have been implemented inside the Karnak.sGbem [26] calculus code, integrated by the MathLab 7.6 program for the solution of the QPP.

The Karnak program, based on the SGBEM formulation, actually permits one in a sub-structuring process to evaluate the elastic and elastoplastic response (displacements, tractions, stresses, strains) of the 2D structures subjected to external actions like body forces and inelastic strains, both in the domain, and also to imposed displacements and to forces at the constrained and free boundary, respectively.

3.1 Contact-detachment by iterative LCP

Let the homogeneous elastic two-dimensional bodies A and B in Fig. 1 both be subjected to imposed displacements $\overline{\mathbf{u}}_1$ on Γ_1, to boundary forces $\overline{\mathbf{f}}_2$ on Γ_2 and to body forces $\overline{\mathbf{b}}$ in Ω. We suppose that friction does not occur between the two bodies and that simple contact or detachment is possible.

Let us introduce the coefficient $c \geq 0$ characterizing the cohesion between the boundaries in contact Γ^A_{0r} and Γ^B_{0r}, in the zone of potential detachment, and the vector modulus $|\boldsymbol{h}| \geq 0$ representing the distances between the corresponding

Author's personal copy

points (reference gap) on the boundary nodes of Γ^A_{0v} and Γ^B_{0v}, in the zone of potential contact.

3.1.1 Continuum approach

Let us denote

- by $\mathbf{t}^A_{0r} = -\mathbf{t}^B_{0r}$ the stress vector acting between the contact points on the real boundaries Γ^A_{0r} and Γ^B_{0r} respectively, $\mathbf{t}^A_{0v} = \mathbf{t}^B_{0v} = \mathbf{0}$ being verified on the virtual boundaries Γ^A_{0v} and Γ^B_{0v},
- by $\mathbf{u}^A_{0v} \neq \mathbf{u}^B_{0v}$ the displacement vectors at the virtual boundaries Γ^A_{0v} and Γ^B_{0v}, $\mathbf{u}^A_{0r} = \mathbf{u}^B_{0r}$ being equal quantities between the displacements of the contact points on the common boundaries Γ^A_{0r} and Γ^B_{0r}.

The boundary conditions of the contact-detachment problem are the following:

$$\mathbf{n}^A \left(\left(\mathbf{u}^A_{0v} - \mathbf{u}^B_{0v} \right) - \boldsymbol{h} \right) \leq 0 \quad c = 0 \quad \text{gap condition} \tag{28a}$$

$$\mathbf{n}^A \, \mathbf{t}^A_{0r} - c \leq 0 \,, \quad \boldsymbol{h} = \mathbf{0} \quad \text{contact condition} \tag{28b}$$

$$\left[\mathbf{n}^A \left(\left(\mathbf{u}^A_{0v} - \mathbf{u}^B_{0v} \right) - \boldsymbol{h} \right) \right] \left[\mathbf{n}^A \, \mathbf{t}^A_{0v} \right] = 0$$
$$\text{complementarity condition on } \Gamma_{0v} \tag{28c}$$

$$\left[\mathbf{n}^A \left(\mathbf{u}^A_{0r} - \mathbf{u}^B_{0r} \right) \right] \left[\mathbf{n}^A \, \mathbf{t}^A_{0r} - c \right] = 0$$
$$\text{complementarity condition on } \Gamma_{0r} \tag{28d}$$

valid at every point on the boundary, where $\mathbf{n}^A$ is the transpose of the normal vector associated with the boundary $\Gamma^A_0 = \Gamma^A_{0r} \cup \Gamma^A_{0v}$ of the body A.

We show the detachment process:

In the boundary zone marked by Γ_{0r}, where the contact between the two bodies occurs ($c>0$, $|\boldsymbol{h}|=0$), the following conditions must be verified: $\mathbf{n}^A \left(\mathbf{u}^A_{0r} - \mathbf{u}^B_{0r} \right) = 0$ and $\mathbf{n}^A \, \mathbf{t}^A_{0r} \leq c$. The detachment phenomenon is checked through the value assumed by the traction $\mathbf{t}^A_{0r}$. Indeed, it occurs when the external action change produces a traction $\mathbf{t}^A_{0r}$ whose value satisfies the condition $\mathbf{n}^A \, \mathbf{t}^A_{0r} \geq c$, c being the limit value. Therefore the latter condition must be considered as the beginning of the detachment process. In this case the point in contact is divided into two points belonging to the bodies A and B and, as a consequence, it causes the rise of the virtual boundaries Γ^A_{0v} and Γ^B_{0v}.

We show the contact process:

Vice versa, in the boundary zone marked by Γ_{0v}, where the contact between the two bodies ($c = 0$, $|\boldsymbol{h}| > 0$) does not exist, the following conditions have to be verified: $\mathbf{n}^A \left(\mathbf{u}^A_{0v} - \mathbf{u}^B_{0v} \right) \leq \mathbf{n}^A \boldsymbol{h}$ and $\mathbf{n}^A \, \mathbf{t}^A_{0v} = 0$. The contact phenomenon is checked through the values assumed by the displacements $\mathbf{u}^A_{0v}$ and $\mathbf{u}^B_{0v}$ of the boundaries Γ^A_{0v} and Γ^B_{0v} of both the bodies: indeed, it occurs when the external action change causes values of the displacements $\mathbf{u}^A_{0v}$ and $\mathbf{u}^B_{0v}$ to satisfy the following condition: $\mathbf{n}^A \left(\mathbf{u}^A_{0v} - \mathbf{u}^B_{0v} \right) \geq \mathbf{n}^A \boldsymbol{h}$, $\boldsymbol{h}$ being the limit vector. Therefore the latter condition must be considered as the beginning of the contact process. In this case the points on Γ^A_{0v} and Γ^B_{0v} become connected at a single point and, as a consequence, this causes the rise of the common contact zone Γ_{0r}.

3.1.2 Discrete approach

Within the topic of the SGBEM, to reach the analytical solution to this frictionless contact-detachment problem, an iterative LCP procedure can be employed once the elastic analysis has been performed using Eq. (23).

To this aim we remember that the unknown vectors $\mathbf{F}_{0r}$, $\mathbf{U}^A_{0v}$ and $\mathbf{U}^B_{0v}$ are referred to the nodes of the in-contact boundary and to the nodes of the detached one. The vector $\mathbf{F}_{0r}$ represents the nodal forces of the body A, computed in the real boundary zone Γ_{0r} and the vectors $\mathbf{U}^A_{0v}$ and $\mathbf{U}^B_{0v}$ represent the nodal displacements of the virtual boundaries of Γ^A_{0v} and Γ^B_{0v}.

With reference to the system of the two in-contact bodies, whose boundaries are discretized into boundary elements, Eqs. (28a–d) characterizing the boundary conditions of the phenomenon being examined can be rewritten in a very similar way. Indeed, the nodal boundary vectors $\mathbf{F}_{0r} = \mathbf{F}^A_{0r} = -\mathbf{F}^B_{0r}$, $\left(-\mathbf{U}^A_{0v}\right)$ and $\left(-\mathbf{U}^B_{0v}\right)$ (changed in sign) must substitute the vectors $\mathbf{t}^A_{0r}$, $\mathbf{u}^A_{0v}$ and $\mathbf{u}^B_{0v}$, the latter being defined at each point on the boundary. Therefore:

$$\mathbf{N}^A_v \left(\left(\mathbf{U}^A_{0v} - \mathbf{U}^B_{0v} \right) - \mathbf{H} \right) \leq \mathbf{0} \,, \quad \mathbf{C} = \mathbf{0} \, \text{gap condition} \tag{29a}$$

$$\mathbf{N}^A_r \, \mathbf{F}_{0r} - \mathbf{C} \leq \mathbf{0} \,, \quad \mathbf{H} = \mathbf{0} \, \text{contact condition} \tag{29b}$$

$$\left[\mathbf{N}^A_v \left(\left(\mathbf{U}^A_{0v} - \mathbf{U}^B_{0v} \right) - \mathbf{H} \right) \right] \left[\mathbf{N}^A_v \, \mathbf{F}_{0v} \right] = 0$$
$$\text{complementarity condition on } \Gamma_{0v} \tag{29c}$$

$$\left[\mathbf{N}^A_r \left(\mathbf{U}^A_{0r} - \mathbf{U}^B_{0r} \right) \right] \left[\mathbf{N}^A_r \, \mathbf{F}_{0r} - \mathbf{C} \right] = 0$$
$$\text{complementarity condition on} \Gamma_{0r} \tag{29d}$$

where $\mathbf{N}^A_r = diag \left(\cdots \, \mathbf{n}^A_i \, \cdots \right)$ and $\mathbf{N}^A_v = diag \left(\cdots \, \mathbf{n}^A_j \, \cdots \right)$ with $i = 1, ...r$ and $j = 1, ...v$.

The vector $\mathbf{H}$ collects all the nodal gaps between the corresponding nodes of the boundaries Γ^A_{0v} and Γ^B_{0v}, in the zone of potential contact, whereas the vector $\mathbf{C}$ collects the cohesion between the nodes which are in contact, in the zone of potential detachment Γ_{0r}.

3.2 Contact-detachment by QPP

The solution to the contact-detachment problem can be obtained as the solution to a *min-max* problem of the functional $\Pi_{rv} \left[\mathbf{F}_{0r}, \, (-\mathbf{U}_{0v}) \right]$ reduced to the nodal interface variables only, as shown by Polizzotto [9] and Polizzotto and Zito

Author's personal copy

[10]. In detail, let us consider the following quadratic problem, whose saddle-point solution is given in the following form:

$$\min_{\mathbf{F}_{0r}} \; - \max_{(-\mathbf{U}_{0v})} \; \Pi_{rv}\left[\mathbf{F}_{0r},\ (-\mathbf{U}_{0v})\right] \quad \text{s.t. } \mathbf{N}_r^A\ \mathbf{F}_{0r} - \mathbf{C} \le \mathbf{0}\ ,\ \ \mathbf{N}_v^A\left(\left(\mathbf{U}_{0v}^A - \mathbf{U}_{0v}^B\right) - \mathbf{H}\right) \le \mathbf{0} \tag{30}$$

with

$$\begin{aligned}\Pi_{rv}\left[\mathbf{F}_{0r}^n,\ \left(-\mathbf{U}_{0v}^n\right)\right] &= \frac{1}{2}\mathbf{Y}_0^T\mathbf{K}_{00}\mathbf{Y}_0 + \mathbf{Y}_0^T\overline{\mathbf{L}}_0 \\ &= \frac{1}{2}\left(\mathbf{F}_{0r}\right)^T\mathbf{K}_{urur}\ \mathbf{F}_{0r} + \left(\mathbf{F}_{0r}\right)^T\mathbf{K}_{urfv}\ \left(-\mathbf{U}_{0v}\right) \\ &\quad + \frac{1}{2}\left(-\mathbf{U}_{0v}\right)^T\mathbf{K}_{fvfv}\ \left(-\mathbf{U}_{0v}\right) \\ &\quad + \left(\mathbf{F}_{0r}\right)^T\overline{\mathbf{L}}_{ur} + \left(-\mathbf{U}_{0v}\right)^T\overline{\mathbf{L}}_{fv}\end{aligned} \tag{31}$$

The QPP problem of Eq. (30) is presented in the classical form of a quadratic objective functional subjected to linear constraints. The saddle-point of this functional provides the complete solution (25) to the contact-detachment problem.

Alternatively, the use of Eq. (26) can modify the *min-max* problem (30) into two separate sub-problems of *min* and *max* of two functionals Π_v and Π_r in order to perform the contact and detachment analysis, independently, as a function of the phenomenon type expected, i.e.

– for the contact problem

$$\max_{(-\mathbf{U}_{0v}^n)} \ \Pi_v\left[(-\mathbf{U}_{0v})\right] \quad \text{s.t. } \mathbf{N}_v^A\left(\left(\mathbf{U}_{0v}^A - \mathbf{U}_{0v}^B\right) - \mathbf{H}\right) \le \mathbf{0} \tag{32a}$$

– for the detachment problem

$$\min_{\mathbf{F}_{0r}} \ \Pi_r\left[\mathbf{F}_{0r}\right] \quad \text{s.t. } \mathbf{N}_r^A\ \mathbf{F}_{0r} - \mathbf{C} \le \mathbf{0} \tag{32b}$$

Π_v and Π_r being two discrete energy forms written in terms of kinematical $(-\mathbf{U}_{0v})$ and mechanical $\mathbf{F}_{0r}$ nodal variables on Γ_{0v} and Γ_{0r} respectively, i.e.

$$\Pi_v\left[(-\mathbf{U}_{0v})\right] = \frac{1}{2}\left(-\mathbf{U}_{0v}\right)^T\tilde{\mathbf{K}}_{fvfv}\ \left(-\mathbf{U}_{0v}\right) + \left(-\mathbf{U}_{0v}\right)^T\tilde{\mathbf{L}}_{fv} \tag{33a}$$

$$\Pi_r\left[\mathbf{F}_{0r}\right] = \frac{1}{2}\left(\mathbf{F}_{0r}\right)^T\tilde{\mathbf{K}}_{urur}\ \mathbf{F}_{0r} + \left(\mathbf{F}_{0r}\right)^T\tilde{\mathbf{L}}_{ur} \tag{33b}$$

These two functionals are alternative to the mixed one given by Eq. (31). Indeed, they are the consequence of the change in Eq. (25), which is modified through variable division, leading to Eq. (26).

In detail, through the maximum problem (32a), all the nodes of the virtual boundary Γ_{0v}, where the condition $\mathbf{N}_v^A\left(\left(\mathbf{U}_{0v}^A - \mathbf{U}_{0v}^B\right) - \mathbf{H}\right) = \mathbf{0}$ occurs, change into the real boundary Γ_{0r}, thus defining a new contact zone. Vice versa through the minimum problem (32b), all the nodes of the real boundary Γ_{0r}, where the condition $\mathbf{N}_r^A\ \mathbf{F}_{0r} - \mathbf{C} = \mathbf{0}$ occurs, change into the virtual boundary Γ_{0v}, thus defining a new detachment zone.

The strategies leading to the solution of the saddle-point of the *min-max* functional (30), of the *min* of the functional (32a) or of the *max* of the functional (32b) do not make it possible to obtain information regarding the evolution of the contact-detachment problem, but only knowledge of the final detachment or contact zones. The advantage is that the functionals have reduced dimensions, thus reducing the computational burden. Once the contact and detached zones are known, it is possible to perform a classical analysis on two bodies whose contact zone is known.

The QP of Eq. (30), or alternatively those of Eqs. (32a, b) are quadratic programming problems not involving computational or mathematic difficulties, because they show a classical form having quadratic objective functions subjected to linear constraints. A strong variable condensation process leads to the writing of algebraic operators only reduced to discrete quantities related to the contact-detachment phenomenon, in a similar way to what was done by Polizzotto [9] and Polizzotto and Zito [10] inside the SGBEM formulation. As a consequence, it was possible to develop the QPP methodology showing a clear mathematic form, because the algebraic operators present in Eqs. (31, 33a, 33b) are symmetric and in sign definite and have reduced dimension. These types of mathematical problems do not need to have solvers and fully-developed quadratic programming techniques like those to be utilized in semi-definite programming. The used implementation strategy coupled the Karnak.sGbem [26] code to obtain the $\mathbf{K}$ matrices and the load vectors $\mathbf{L}$ with MathLab 7.6, which provides the solution of the QPP Eqs. (30, 32a, 32b). The QPP (32a,b) can be utilized singularly in cases of detachment or contact only, or in the alternative strategy where these two phenomena coexist.

The present paper works in the ambit of the matching mesh, but some explanations regarding the implementation strategy used to transfom an imperfectly matching mesh into a perfectly matching mesh have to be shown. Indeed, when the phenomenon regards the potential detachment Γ_{0r}, certainly we are in the presence of a perfectly matching mesh. Vice versa, when the phenomenon contemplates contact presence on Γ_{0v} the nodes would not guarantee a perfectly matching mesh during the contact phase. To this aim a simple recursive strategy was implemented which modifies the discretization to very few iterations (2 or 3) and leads to a perfectly matching mesh, by changing the position of the nodes belonging to only one of the two bodies.

Author's personal copy

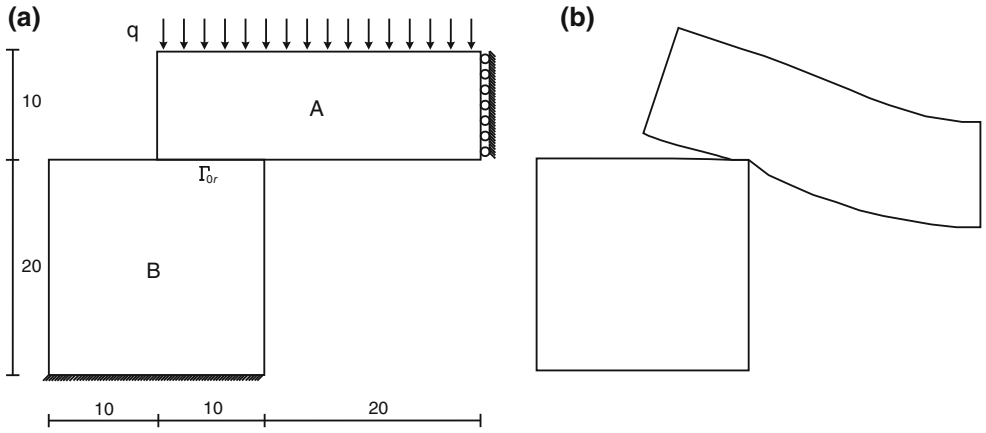

Fig. 2 Beam supported on elastic blocks: **a** geometric description, **b** strained shape obtained by iterative LCP analysis

Table 1 Comparison of detachment lengths and CPU times

Method	Detachment length (cm)	CPU times (s)
SGBEM iterative LCP	8.4	237.7
BEM (R. Vodička [14])	8.3	//
SGBEM QPP	8.2	4.3

4 Numerical applications

To show the efficiency of the proposed methods, some structures were analyzed. These were subjected to external actions, constant in time. In the first two examples, the detachment phenomenon is treated by iterative LCP and QPP procedures in the absence of cohesion between the substructures and in the absence of friction and sliding, and a comparison is made between these two different approaches. The last example was treated in the presence of different cohesion values, but only through an LCP analysis.

4.1 Example 1

Let us consider the detachment problem regarding a beam A supported by two elastic blocks B, without friction and sliding, and symmetrically loaded. The analysis is performed on half the structure, as shown in Fig. 2a.

The geometrical and mechanical characteristics of the structure are the same as those utilized by Vodička [14]. Thus the beam A, having unitary thickness, is characterized by the Young modulus $E_a = 30.6 \times 10^4$ MPa and Poisson ratio $\upsilon = 0.3$ and is subjected to vertical force distribution $q = 1020$ daN/m. The body B is characterized by the Young modulus $E_b = 30.6 \times 10^6$ MPa and by the same thickness and Poisson coefficient.

To discretize the free and constrained boundaries of the solids A and B, a step $p = 2$ cm was introduced on Γ_2 and Γ_1, whereas to discretize the contact boundary Γ_{0r} the step $p = 0.1$ cm was utilized. Figure 2b shows the final strained shape obtained by the iterative LCP.

In Table 1 the detachment length is shown, computed using the strategies in Sects. 3.1 and 3.2. These results were compared with the solution obtained by Vodička [14]. In all the cases shown in Table 1 the detachment length proves to be very similar. The same table also shows the CPU times employed by the two strategies, proving that the QPP methodology gives a drastic reduction in CPU times.

Figure 3a, b show the normal and shear stress distributions in the transversal sections of the bodies A and

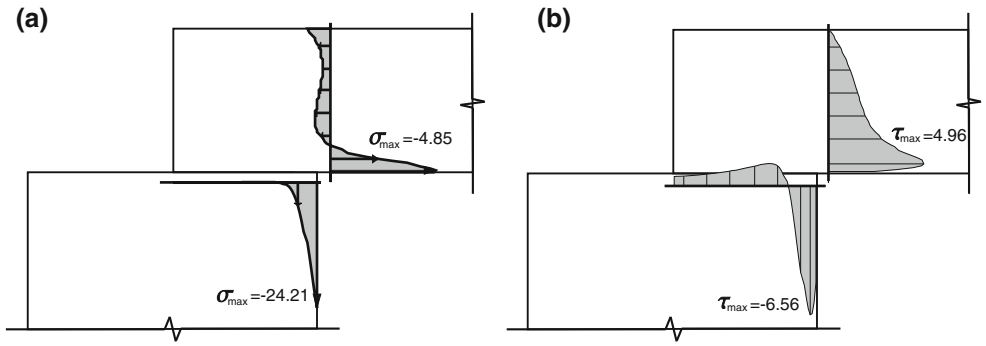

Fig. 3 **a** Normal and **b** shear stress distributions.

Author's personal copy

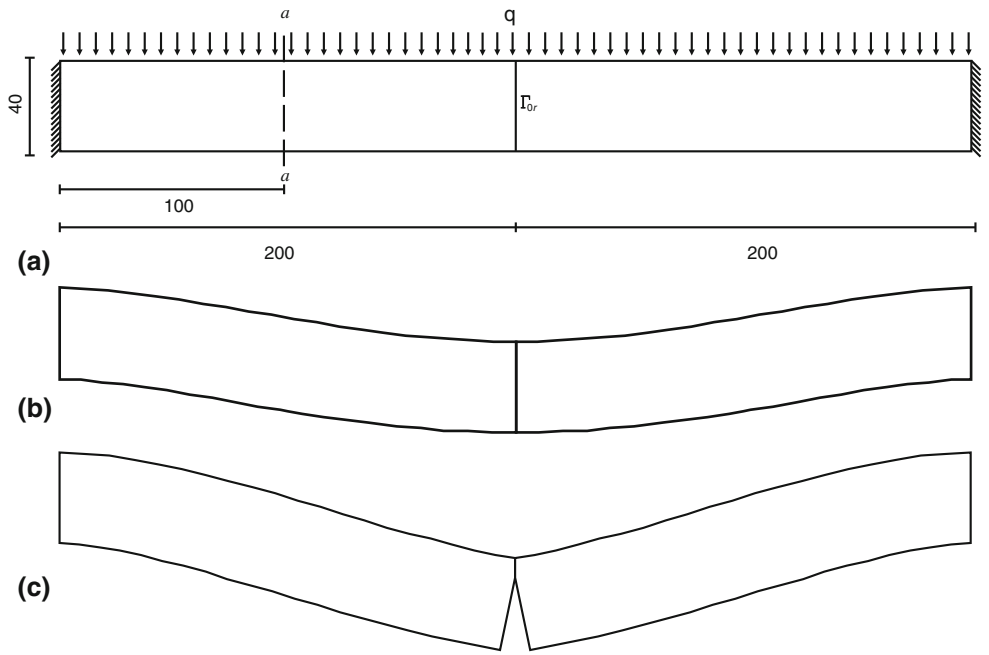

Fig. 4 Double constrained beam: **a** geometric description, **b** strained shape by elastic analysis without detachment, **c** strained shape by iterative LCP analysis considering the detachment phenomenon

B, distant 1 cm from the inner corner between A and B, obtained at the end of the iterative LCP analysis. This stress state, but also other kinematical and mechanical characteristics, such as displacements, relative displacements, strains and support reactions, can be known by utilizing the peculiarities of the Karnak program. The latter information is not obtainable when we use the QPP methodology, which is an alternative to LCP.

4.2 Example 2

In Fig. 4a a double constrained beam, having unitary thickness, is subjected to a vertical load $q = 1000\,\text{daN/m}$. The material characteristics are: Young's modulus $E = 5000\,\text{MPa}$ and Poisson's ratio $\upsilon = 0.2$. To discretize the free Γ_2 and constrained Γ_1 boundaries of the solids A and B, nodes with step $p = 4\,\text{cm}$ were introduced everywhere, whereas to discretize the contact boundary Γ_{0r} the step $p = 0.38\,\text{cm}$ was utilized, thus introducing 104 nodes along the interface.

For this beam, three analyses were performed:

- an elastic analysis, carried out with the Karnak program, considering the beam as continuous without possibility of detachment and comparing the elastic response with the analytical solution to the monodimensional solid;
- a nonlinear analysis, carried out with the Karnak program, to evaluate the detachment length through an iterative LCP approach, following the strategy introduced in Sect. 3.1;
- a nonlinear analysis, carried out with the Karnak program and coupled with the MathLab code, to evaluate the detachment length through a QPP approach, following the strategy shown in Sect. 3.2.

Table 2 Comparison of detachment lengths and CPU times

Method	Detachment length (cm)	CPU Times (s)
SGBEM iterative LCP	33.85	984.4
SGBEM QPP	33.08	16.2

In Fig. 4 the strained shapes obtained by elastic analysis (Fig. 4b) and by the iterative LCP (Fig. 4c) are shown.

In Table 2 the detachment length is shown, which was computed using the strategies of the Sects. 3.1 and 3.2. In both cases the detachment lengths prove to be similar and show an error equal to 2.27 %. The same table also shows the CPU times employed by the two strategies, proving that the QPP methodology leads to a drastic reduction in CPU times.

In Fig. 5 the normal stress σ_x and the shear stress τ_{xy}, obtained at the section a–a distant 100 cm from the left built-in end section, are compared by considering three analysis types, i.e. continuum beam theory, continuum beam by Karnak program and iterative analysis by Karnak program with detachment at the final step.

It is possible to show the development of the phenomenon through LCP iterative analysis using the Karnak program. For instance, we want to evaluate the normal stress in the section a–a when the detached boundary takes on the value

Author's personal copy

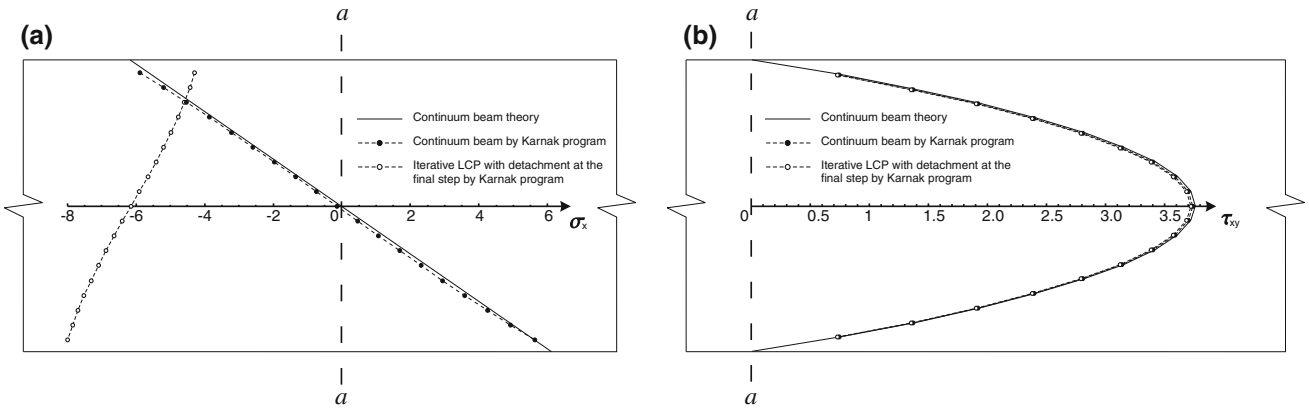

Fig. 5 Stress distribution at the section *a–a*: **a** normal stress σ_x and **b** shear stress τ_{xy}

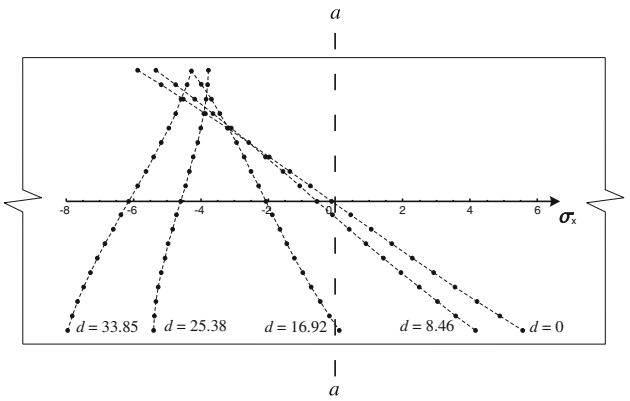

Fig. 6 Normal stress distribution σ_x at section *a–a* during the detached phenomenon

expressed in cm, i.e. $d = 0.00, 8.46, 16.92, 25.38, 33.85$. It can be noticed that the detachment modifies the response in terms of normal stress σ_x, losing its linearity and reaching only negative values when the detachment length takes on the value d= 16.92, as shown in Fig. 6. Vice versa the shear stress τ_{xy} remains unchanged because, in this case, the shear is not influenced by the detachment process (Fig. 5b).

As a conclusion to the two examples, some observations have to be introduced.

In analyzing the differences found in the two applications between the LCP and QPP solutions, the percentage error (2.3 % in the first example, 2.2 % in the second one) are acceptable, but it is necessary to explain these differences. In this connection, the QPP strategy shows a direct approach where the solution of a stationary problem is performed, all the data being known at the beginning through the knowledge of the algebraic operators. By contrast, the LCP strategy is an indirect approach, based on the search of the solution of an evolutive problem, in which at every iteration of the contact-detachment process the problem is modified as we move towards the stationary solution.

As a consequence the solutions obtained through a direct (QQP) and an indirect (LCP) approach are not perfectly coincident, mainly for three reasons:

- the first one is connected to the check type introduced in deciding to proceed with or exit from the iterative process. This check defines an error range involving a response variation and modifies the conditions of the beginning of the new iterative step with new modified operators;
- the second one is connected to the modelling of the boundary quantities in the contact-detachment zone. Indeed, at the end of the iterative process, the presence of high stress concentrations means that the tractions, as well as the relative displacements, are not fairly represented by the linear shape functions, which are introduced both to perform the cause modelling and the effect weighting;
- the third one regards the strategy employed during the contact process. In this connection, the direct QQP procedure does not modify the mesh during the characterization

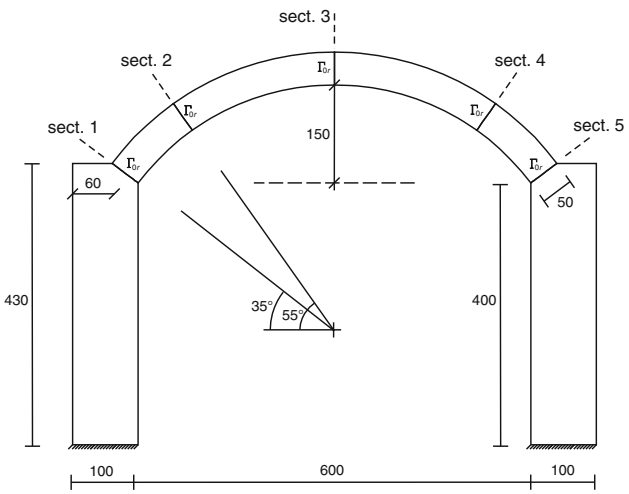

Fig. 7 Geometry of a vault supported by quasi-rigid blocks

Author's personal copy

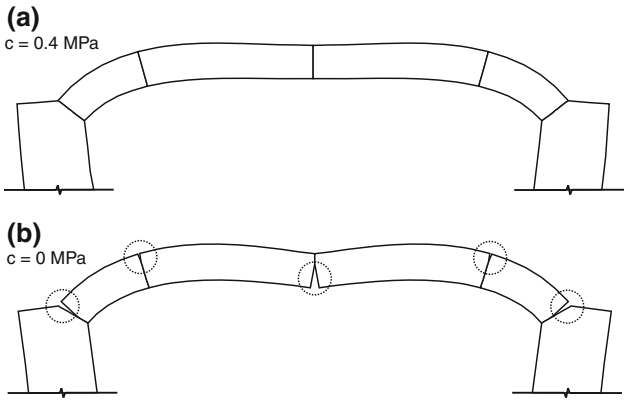

Fig. 8 Strained shapes by iterative LCP analysis: **a** with cohesion $c = 0.4$, **b** with cohesion $c = 0$

Table 3 Detachment lengths by iterative LCP for different coesion values $c = 0.4, \ldots, 0$ MPa

	Detachment length (cm) with different cohesion values (MPa)				
Sections	$c = 0.4$	$c = 0.3$	$c = 0.2$	$c = 0.1$	$c = 0$
1–5	0	35.29	35.29	35.29	35.29
2–4	0	0	0	0	11.76
3	0	0	0	38.24	38.24

of the contact zone, as instead it happens in the iterative LCP procedure.

4.3 Example 3

Let us consider the frictionless detachment phenomenon, without sliding, in Fig. 7, where a depressed vault is supported on two quasi-rigid masonries. The vault/masonry system was discretized by 6 substructures, 4 of which BEM-e ones for the vault and 2 BEM-e ones for the support masonry. The system is subjected to its own weight. The vault, having Young modulus $E = 7500$ MPa, Poisson ratio $\upsilon = 0.3$ and thickness $s = 100$ cm, is subjected to the body force $\gamma = 1800$ daN/m^3. The support masonries, constrained at the bases, are characterized by the same thickness, Poisson ratio and body force as the vault, but have a different Young modulus $E = 25000$ MPa.

Table 4 Maximum stress values by iterative LCP for cohesion values $c = 0.4, 0.0$ MPa

	Maximum stress values (MPa)	
Sections	$c = 0.4$	$c = 0$
1–5	−0.39674	−0.49140
2–4	−0.16843	−0.16372
3	−0.20383	−0.33641

Five sections (Fig. 7) characterizing the interface boundaries between substructures were introduced to simulate the separation phenomenon through the use of the iterative LCP strategy shown in Sect. 3.1 with different cohesion values $c = 0.4, 0.3, 0.2, 0.1, 0.0$ MPa. Each section contains 18 interface nodes.

By the analysis performed through the strategy developed in Sect. 3.1, it is shown that for the cohesion value equal to $c = 0.4$ MPa no section is subjected to the detachment phenomenon. By contrast, when the cohesion is null, all the sections are subjected to a separation process, but having different detachment lengths. In Fig. 8 the strained shapes related to the two limit values of cohesion $c = 0.4$ and $c = 0$ are shown.

In Table 3 the detachment lengths obtained by the employed cohesion values are indicated.

In the presence ($c = 0.4$ MPa) and in the absence of cohesion, the detachment process involves the compression stress being concentrated in the in-contact zone, and at the same time the traction stress disappears near the detached interface boundary. These results are shown in Fig. 9, where the normal stress distribution has been drawn near the sections

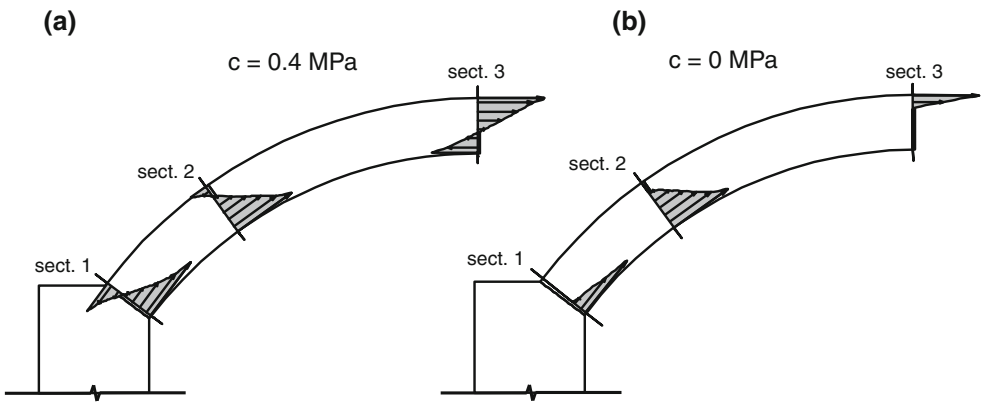

Fig. 9 Normal stress distributions by iterative LCP analysis for cohesion values $c = 0.4, 0.0$ MPa

Author's personal copy

introduced to study the detachment phenomenon. At the end, Table 4 shows the maximum stress values in the presence ($c = 0.4$ MPa) and in the absence of cohesion.

5 Conclusions

In the hypothesis of absence of friction and sliding, the contact-detachment phenomenon between two elastic bodies was obtained through an iterative LCP strategy and through a QPP procedure, using the SGBEM for multidomain problems. A boundary discretization was made, producing a symmetric formulation where the displacements and the tractions are introduced in terms of discrete quantities (nodal displacements and forces). In both the strategies used, the minimum reference gap and the cohesion have to be known.

The iterative LCP strategy is computationally disadvantageous, but allows one to have a lot of information regarding the status of the body, that is regarding displacements, normal and shear stresses, normal and shear strains, distribution of displacements and stresses along prefixed lines, in any phase of the contact-detachment phenomenon.

By contrast, the QPP procedure uses reduced functionals in terms of nodal displacements and reactions along the interface boundary. It is computationally advantageous, but one only obtains the final value of the contact or detachment boundary and no other information on the status of the bodies.

These two strategies made it possible to activate a modulus in the Karnak.sGbem program through the formulation of appropriate procedures.

References

1. Signorini A (1933) Sopra alcune questioni di elastostatica. Atti della Societa Italiana per il Progresso della Scienza
2. Gwinner J, Stephan EP (1993) A boundary element procedure for contact problems in linear elastostatic. RAIRO Math Model Numer Anal 27:457–480
3. Cottle W, Pang JS, Stone RE (1992) The linear complementarity problem. Academic Press, Boston
4. Xu BQ, Kong XA (1996) A modified tree search algorithm for contact BEM-LCP approach. Comput Struct 59:707–713
5. Panzeca T, Salerno M, Terravecchia S, Zito L (2008) The symmetric boundary element method for unilateral contact problems. Comput Methods Appl Mech Eng 197:2667–2679
6. Shougui Zhang, Jialin Zhu (2012) The boundary element-linear complementarity method for the Signorini problem. Eng Anal Bound Elem 36:112–117
7. Gakwaya A, Lambert D, Cordon A (1992) A boundary element and mathematical programming approach for frictional contact problems. Comput Struct 42:341
8. Maier G, Novati G, Cen Z (1993) Symmetric Galerkin BEM for quasi-brittle fracture and frictional contact problems. Comput Mech 13:74–89
9. Polizzotto C (1993) Variational boundary-integral-equation approach to unilateral contact problems in elasticity. Comput Mech 13:100–115
10. Polizzotto C, Zito M (1998) BIEM-based variational principles for elastoplasticity with unilateral contact boundary condition. Eng Anal Bound Elem 21:329–338
11. Su RKL, Zhu Y, Leung AYT (2002) Parametric quadratic programming method for elastic contact fracture analysis. Int J Fract 117:143–157
12. Oysu C, Fenner RT (2006) Coupled FEM-BEM for elastoplastic contact problems using Lagrange multipliers. Appl Math Model 30:231–247
13. Dostàl Z, Friedlander A, Santos A, Malik J (1996) Analysis of semicoercive contact problems using symmetric BEM and augmented Lagrangians. Eng Anal Bound Elem 18:195–201
14. Vodička R (2000) The first and the second-kind boundary integral equation systems for solution of frictionless contact problems. Eng Anal Bound Elem 24:407–426
15. Eck C, Steinbach O, Wendland WL (1999) A symmetric boundary element method for contact problems with friction. Math Comput Simul 50:43–61
16. Vodička R, Mantič V, París F (2011) Two variational formulation for elastic domain decomposition solved by SGBEM enforcing coupling conditions in weak form. Eng Anal Bound Elem 35: 148–155
17. Perez-Gavilan JJ, Aliabadi MH (2001) A symmetric Galerkin BEM for Multi-connected bodies: a new approach. Eng Anal Bound Elem 25:633–638
18. Maier G, Diligenti M, Carini A (1991) A variational approach to boundary element elastodynamic analysis and extension to multidomain problems. Comput Methods Appl Mech Eng 92:192–213
19. Gray LJ, Paulino GH (1997) Symmetric Galerkin boundary integral formulation for interface and multi-zone problems. Int J Numer Methods Eng 40:3085–3101
20. Layton JB, Ganguly S, Balakrishna C, Kane JH (1997) A symmetric Galerkin multi-zone boundary element formulation. Int J Numer Methods Eng 40:2913–2931
21. Ganguly S, Layton JB, Balakrishna C, Kane JH (1999) A fully symmetric multi-zone Galerkin boundary element method. Int J Numer Methods Eng 44:991–1009
22. Panzeca T, Salerno M (2000) Macro-elements in the mixed boundary value problems. Comput Mech 26:437–446
23. Maier G, Polizzotto C. (1987) A Galerkin approach to boundary element elastoplastic analysis. Comput Methods Appl Mech Eng 60:175–194
24. Maier G, Polizzotto C (1987) A Galerkin approach to boundary element elastoplastic analysis. Comput Methods Appl Mech Eng 60:175–194
25. Terravecchia S (2006) Closed form coefficients in the symmetric boundary element approach. Eng Anal Bound Elem 30:479–488
26. Cucco F, Panzeca T, Terravecchia S (2002) The program Karnak. sGbem, Release 2.1